A far-infrared Fourier transform spectrometer with an antenna-coupled niobium bolometer

D F Santavicca, A J Annunziata, M O Reese, L Frunzio and D E Prober

Department of Applied Physics, Yale University, New Haven, CT 06520-8284, USA

E-mail: daniel.santavicca@yale.edu and daniel.prober@yale.edu

Abstract
We have designed and constructed a custom far-infrared Fourier transform spectrometer using an antenna-coupled bolometer as a detector. The active element of the detector is a superconducting niobium microbridge, and the far-infrared signal is coupled to the microbridge via a planar antenna mounted on a hyperhemispherical silicon lens. The spectrometer uses a broadband blackbody source with frequency-independent optical components, and thus the system bandwidth is set by the detector antenna. We have fabricated devices with two different antenna types, the double dipole and the log spiral, and have characterized the spectral response of each. This spectrometer can utilize the fast response of the niobium bolometer to perform time-resolved far-infrared spectroscopy on nanosecond to millisecond timescales. These timescales are too fast for standard commercial bolometers and too long for a typical optical delay line.

1. Introduction

Far-infrared (FIR) or terahertz (THz) spectroscopy is an important tool for molecular characterization, as many light molecules have vibrational, rotational and torsional modes in this spectral range. Additionally, FIR spectroscopy is a sensitive probe of solid state materials, as it can be used to measure lattice modes and the motion of mobile charges. It is especially useful as a non-contact probe for studies of nanoscale systems, where attaching electrical leads is problematic. Biological systems are also amenable to FIR studies, such as measuring the low frequency motions of proteins [1]. The present paper provides an initial demonstration of the feasibility of a niobium (Nb) microbolometer for such spectroscopy applications.

The two standard techniques for these types of studies are THz time-domain spectroscopy (TDS) and FIR Fourier transform spectroscopy (FTS). TDS was developed in the late-1980s following the discovery that a coplanar stripline on a semiconducting substrate, when exposed to an ultra-fast laser pulse, will radiate into free space with an output bandwidth limited by the envelope of the laser pulse [2]. A similar coplanar stripline device can be used as a detector, which is synchronized with the same optical pulse used to drive the emitter [3]. This technique and its variants are now utilized by many research groups and can achieve bandwidths of several THz with high signal-to-noise ratios and peak power $\sim$mW [4]. By using the same optical pulse to excite a sample and varying the time delay between the excitation pulse and the pulse on the detector, one can perform dynamic measurements of the emitted electric field with sub-picosecond time resolution [1]. This is often referred to as time-resolved THz spectroscopy (TRTS) to distinguish it from standard THz TDS. The upper time limit of this technique is set by the length of the optical delay line, which typically corresponds to a maximum timescale of the order of a nanosecond.

FTS uses a blackbody source such as a mercury arc lamp or heated filament. These sources are more broadband than the sources of TDS but have much lower peak power. The time resolution in FTS is set by the response time of the detector. The most common detector type is the silicon (Si) bolometer, which has a thermal time constant $\tau \sim$ ms and an optical noise equivalent power (NEP) of 2×10^{-12} W (Hz)$^{-1/2}$ at 4.2 K [5]. Faster options include the gallium-doped germanium photoconductive detector ($\tau \sim 1$ μs, NEP $\sim 10^{-12}$ W (Hz)$^{-1/2}$) and the indium antimonide bolometer

($\tau \sim 100$ ns, NEP $\sim 10^{-12}$ W (Hz)$^{-1/2}$) [5]. These have a more limited input bandwidth than the slower Si bolometer. All of these detectors measure power, unlike TDS, which measures electric field. They are all large-area, multi-mode detectors which typically use a Winston cone to couple the incident signal to the device. Because of their slow time constant, these detectors are usually used in FTS to study samples whose properties are constant in time.

We have developed a superconducting bolometric detector that is significantly faster than conventional bolometers, and we have integrated this detector into a custom spectrometer. This system is designed to bridge the gap in time resolution between TRTS and present versions of FTS that employ a standard commercial detector. The active element of our detector is a Nb microbridge and the incident FIR signal is coupled to the microbridge with a planar aluminum (Al) antenna mounted on a hyperhemispherical Si lens. The response time is set by electron–phonon coupling in the Nb film, measured to be 0.7 ns at 6 K. An optimum responsivity of 4.4×10^4 V W^{-1} is obtained at a bath temperature $\approx 0.9 T_c$, where T_c is approximately 6 K. The measured electrical NEP referred to the detector is 2.0×10^{-14} W (Hz)$^{-1/2}$, near the thermal fluctuation NEP inferred from the thermal conductance. The output noise is white from approximately 100 Hz to 100 MHz. The saturation power corresponding to the optimum responsivity is 7 nW. Lowering the bath temperature increases the saturation power but decreases the responsivity. A detailed discussion of the device characteristics can be found in [6].

With low inductance and negligible stray capacitance, a short ($\sim \mu$m) Nb microbridge is an efficient absorber up to ~ 10 THz. In this case, the frequency range of the detector is set by the antenna bandwidth. When employed in a spectrometer with optics that are frequency-independent over the relevant spectral range, the entire system bandwidth is set by the antenna. We have fabricated and measured devices with multiple antenna geometries. These different geometries will allow a user to select an input bandwidth that is optimized for a particular application. Devices with four different antenna geometries are pictured in figure 1.

Previous work by Gershenzon *et al* studied the response of large-area Nb devices to infrared radiation [7]. These devices consisted of two geometries, a meander pattern and a series of parallel strips. Because of the large area of each design (area $\gg \lambda^2$), coupling to the device was achieved without a substrate lens or antenna. More recently, a commercial bolometer consisting of a 3×3 mm^2 Nb film has been developed by QMC Instruments at Cardiff University [5]. This detector has a similar response time to our devices, but with significantly poorer sensitivity, with a quoted optical NEP of 1×10^{-10} W (Hz)$^{-1/2}$. By minimizing the detector volume, our device achieves much better sensitivity than a large-area detector. Additionally, a planar antenna couples to photons of a single mode, collecting much less background power than a large-area, multi-mode detector. The antenna-coupled superconducting microbolometer has been developed extensively over the past decade as a low-noise mixer for radioastronomy applications [8] but has not previously been used as a direct detector for lab spectroscopy.

Insight Product Co. and the Gol'tsman group at Moscow State Pedagogical University have recently developed a similar
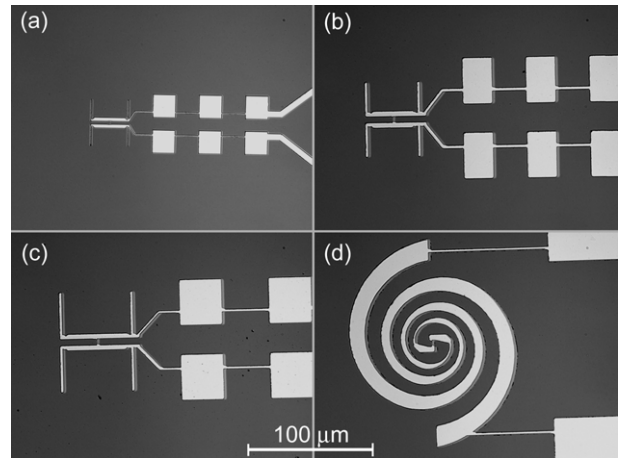

Figure 1. Optical images of devices with different antenna geometries: (a) 38 μm double dipole, (b) 59 μm double dipole, (c) 79 μm double dipole, (d) log spiral. The Nb microbridge is located at the center of each antenna and leads with quarter-wave THz choke structure are visible to the right. All images are at the same magnification.

Nb direct detector with a log periodic antenna for the spectral range 0.3–3 THz. The quoted response time is 1 ns and the quoted optical NEP is 5–7×10^{-14} W (Hz)$^{-1/2}$ [9]. The details of the measurement, such as the modulation frequencies at which the stated NEP is valid, are not specified. We expect this device to have similar performance to the devices described in [6]. Insight also offers a niobium nitride detector for the same spectral range that is an order of magnitude faster but with an order of magnitude poorer sensitivity [9].

We report here the antenna and system characterization. Ultimately, the goal is to use this system to study FIR dynamics. To perform such time-resolved measurements, a sample can be excited with an optical pulse and the THz transmission through the sample can be monitored in real time by measuring the device response using an averaging oscilloscope. A mechanical chopper is not needed. This technique assumes that the laser pulses and the sample response are highly reproducible. The frequency-averaged THz transmission as a function of time can be monitored without use of the interferometer. Alternatively, the interferometer can be used to measure the time-dependent transmission at each point in the interferogram. This will give the time dependence of each spectral component.

2. Device fabrication

Devices were fabricated on 200 μm thick, double side polished, high resistivity (>20 kΩ cm) silicon wafers. Device (a) was patterned with e-beam lithography using a single layer of ~ 1 μm thick PMMA A8 950 K and has nominal bridge dimensions of 1 μm $\times$ 2.5 μm $\times$ 12 nm. This is the same device reported in [6]. Devices (b), (c) and (d) were patterned with optical lithography using a single layer of 2.7 μm thick Shipley 1827 photoresist. Following exposure and development, the wafer was placed in a Kurt J Lesker ultra-high vacuum sputter deposition system with a base pressure of 8×10^{-9} Torr. The wafer was cleaned with a neutralized

argon ion beam with a current density of 240 μA cm^{-2} for 30 s, followed by dc magnetron sputtering of approximately 12 nm of Nb from a direction normal to the substrate. This was done at 350 W with an argon pressure of 1.3×10^{-3} Torr. Without breaking vacuum, this was followed by thermal evaporation of 200 nm of Al at an angle of 40° from the substrate normal. The angled deposition covers the antenna and lead structure but does not cover the narrow microbridge, and produces the shadowing effect that is seen in figure 1. (On the right side of the Al pattern, a dark gray band of Nb is visible, approximately the same width as the microbridge.) The optically patterned devices have nominal bridge dimensions of 2 μm $\times$ 5 μm $\times$ 12 nm. This is four times the volume of device (a). The saturation power (P_{sat}) should scale linearly with the volume and the thermal fluctuation NEP should scale with the square root of the volume. P_{sat} and the NEP have been measured fully for device (a) [6]. These quantities will be tested for the larger, optically patterned devices in future measurements. In all devices, the microbridge is designed to have an impedance of 50–100 Ω for detected photons. A quarter-wave choke structure (visible to the right of each device in figure 1) allows dc biasing and dc-rf readout, but is designed to minimize loss of the incident FIR signal.

3. Spectrometer design

Devices are mounted on the back of a double-side patterned alignment piece made from the same high-resistivity silicon used for the device substrate. The device is at the silicon–air interface. On the reverse of the alignment piece, a 6 mm diameter hyperhemispherical silicon lens is attached[1]. We estimate that the alignment accuracy is within ± 10 μm. The device is mounted in an optical-access, continuous-flow ^{4}He cryostat in which the temperature can be adjusted above 4.2 K with a simple resistive heater. The cryostat window consists of a 90 μm thick mylar sheet. A cooled Zitex G110 membrane, which absorbs strongly above 4 THz, is used as an infrared filter on the heat shield window [10].

A schematic of the spectrometer is presented in figure 2. The source is a silicon carbide globar, which reaches a maximum nominal temperature of 1800 °F at a bias voltage of 24 V.[2] We use a 6 mm diameter iris to define the source. The size of this aperture sets a lower frequency limit of $\sim$100 GHz [11]. The blackbody signal from the source is collimated with a 63.5 mm diameter 90° off-axis parabolic mirror. The beamsplitter consists of a 6 mm thick, 100 mm diameter high-resistivity silicon wafer[3]. This has better efficiency and broader spectral coverage than a typical mylar beamsplitter. The etalon spacing is about 7 GHz and the etalon is averaged for frequency resolutions larger than approximately twice this spacing [12].

The scanning mirror is mounted on a linear translation stage controlled by an Ealing EncoderDriver linear actuator. It has a range of motion of 10 mm with a linear resolution of 0.02 μm and a repeatability of 0.1 μm. This range
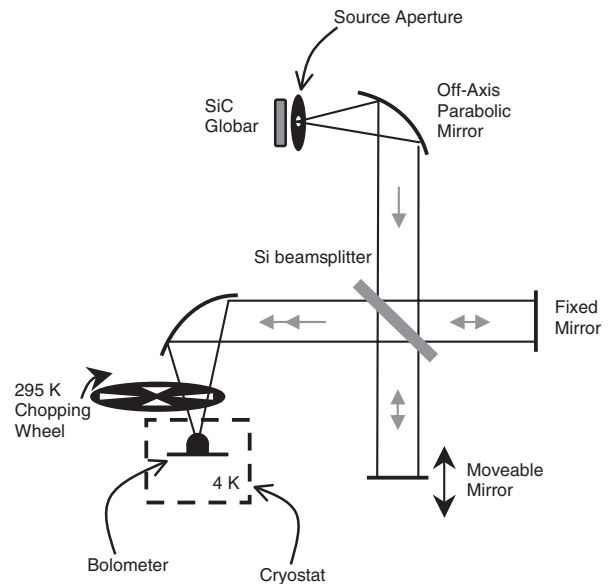
Figure 2. Schematic of the Fourier transform spectrometer.

corresponds to a frequency resolution of 15 GHz. The combined signal from the two arms is focused onto the detector with a second parabolic mirror. We note that none of the optical components should have any significant frequency dependence below 3 THz. Thus, our assumption that the system bandwidth is set by the antenna bandwidth should be valid. A mechanical chopper with a maximum chopping rate of 400 Hz is positioned in front of the cryostat window. The entire system sits inside a nitrogen drybox to minimize absorption from atmospheric water. Flushing with dry nitrogen overnight yields a relative humidity of 2–4%.

The device response at the chopping frequency is amplified by a SR560 low noise voltage preamplifier. A 1:60 transformer at the preamp input steps up the device impedance to achieve optimum noise performance. The device is biased with a 20 Ω dc voltage bias. A large inductor is used on the dc biasing line to minimize noise from the biasing circuit. The output of the preamp is coupled to a lock-in amplifier, which is locked to the chopping frequency.

4. Antenna characterization

The double dipole antenna is designed such that the two half-wave dipole elements radiate in-phase in the direction perpendicular to the substrate but out-of-phase in the direction parallel to the substrate [13]. The antenna radiates power preferentially into the high dielectric silicon in proportion to the square root of the dielectric constant [14], so approximately 80% of the power should be coupled via the hyperhemispherical silicon lens.

The log spiral is part of a class of antennas known as frequency-independent, whose shape is completely specified by angles [15]. The shape of the log spiral is defined in polar coordinates by the equation $\rho = k e^{a(\phi + \phi_0)}$, where k and a are positive constants [16]. In our design, $a = 0.15$. Each arm in the log spiral antenna is formed by the space between
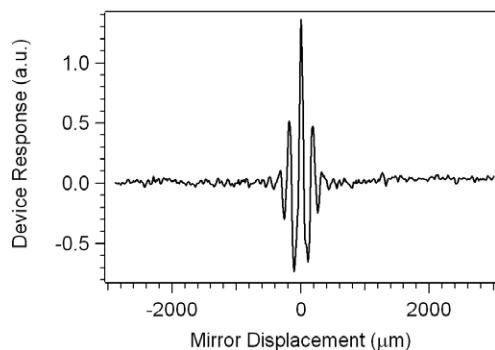
Figure 3. Typical interferogram of device with 79 μm double dipole antenna.

Table 1. Comparison of calculated and fitted dipole resonances

Dipole length (μm)	Calculated center frequency (THz)	Fitted center frequency (THz)
79	0.75	0.80
59	1.00	0.98
38	1.55	1.57

two curves shifted by some angle ϕ_0. Our design is self-complimentary, in which the shift defining each arm is $\pi/2$ and the shift between arms is π. For a finite size antenna, the lower frequency bound corresponds approximately to the wavelength equal to the total arm length, while the upper bound is set by the finite size of the load [16].

The spectrometer has been used to measure the response of the four antenna geometries pictured in figure 1. Typical scans used a step size of 10 μm, corresponding to a frequency range of 7.5 THz, with a time per step of 0.8 s and a lock-in time constant of 300 ms. Scans for all devices were performed at 2–4% relative humidity. A typical scan for device (c), the 79 μm double dipole antenna, is seen in figure 3. The scan length of 6 mm corresponds to a frequency resolution of 25 GHz. It takes approximately 8 min to acquire the data.

The measured interferogram is Fourier-transformed to get the spectral response. Normalized spectra from all four antennas are presented in figure 4. The irregular structure in each spectrum is highly reproducible from scan to scan and thus does not appear to be dominated by noise. The main response peak in each double dipole spectrum was fit with a simple Gaussian to extract a center frequency. This frequency was compared to the calculated half-wave resonance of a dipole of the same physical length in an effective dielectric equal to the mean of the dielectric of silicon ($\varepsilon = 11.9$) and air [14]. These results are compared in table 1. The peak response scales inversely with the antenna linear dimension, as expected. We note that the quantitative agreement with the fitted center frequency may be fortuitous.

The log spiral antenna has a roll-on at $\approx$0.3 THz, consistent with the guideline that the largest wavelength will correspond approximately to the arm length [15], where the wavelength is assumed to be in an effective dielectric that is the mean of the dielectric constants of silicon and air, as before. If a 5 μm microbridge can be assumed to look point-like for wavelengths larger than 8 times its length, the
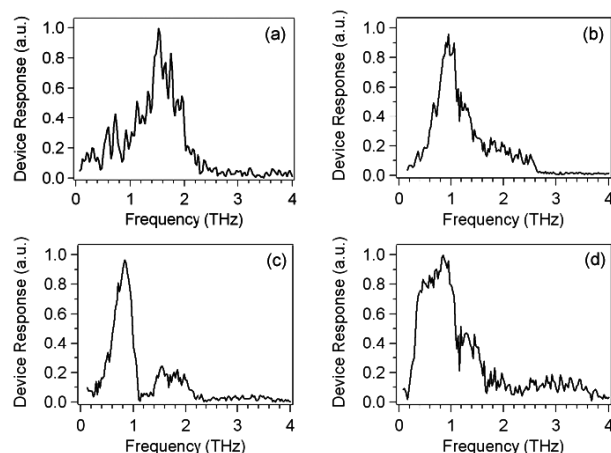

Figure 4. Normalized spectra from each of the four antenna geometries: (a) 38 μm double dipole, (b) 59 μm double dipole, (c) 79 μm double dipole, (d) log spiral.

upper bound of the antenna response should be $\approx$3 THz. At these frequencies, the inductance of the bridge must also be considered. The microbridge inductance of the optically patterned devices is approximately 5 pH, which contributes to the device impedance about j30 Ω/THz. The decrease of power coupling efficiency at 3 THz is approximately 25%.

The attenuation in the measured log spiral response above 1 THz is much greater than the predicted loss due to the device inductance. This may be caused by distortion of the antenna geometry due to the thin film shadowing effect from our angled deposition process. This is seen as the gray band to the right of the Al patterns in figure 1. The minimum shadow size is equal to the width of the microbridge, in this case 2 μm. This shadowing becomes more significant as the spiral width decreases, causing increasing distortion at higher frequencies. This effect can be minimized in future devices by decreasing the width of the microbridge, which allows the use of a thinner resist. To keep the same device resistance, we must maintain the same aspect ratio for a given film thickness, which requires also decreasing the microbridge length. This has the additional benefit of decreasing the inductance.

5. Conclusion

We have demonstrated an antenna-coupled niobium bolometer integrated into a custom FIR spectrometer. This system can be used to study a variety of time-dependent phenomena. Previous work has used TRTS to study time-dependent photoconductivity on picosecond–nanosecond timescales in bulk semiconductors and in ensembles of semiconductor nanoparticles [17–19]. Our system enables the extension of these measurements to longer timescales. Other potential applications include investigations of phonon relaxation [20] and the transient dynamics of protein folding [21]. These applications can all utilize the fast response and high sensitivity of the antenna-coupled niobium bolometer.

References

[1] Beard M C, Turner G M and Schmuttenmaer C A 2002 Terahertz spectroscopy *J. Phys. Chem.* B **106** 7146–59

[2] Smith P R, Auston D H and Nuss M C 1988 Subpicosecond photoconducting dipole antennas *IEEE J. Quantum Electron.* **24** 255–60

[3] van Exter M and Grischkowsky D R 1990 Characterization of an optoelectronic terahertz beam system *IEEE Trans. Microw. Theory Tech.* **38** 1684–91

[4] Han P Y, Tani M, Usami M, Kono S, Kersting R and Zhang X C 2001 A direct comparison between terahertz time-domain spectroscopy and far-infrared Fourier transform spectroscopy *J. Appl. Phys.* **89** 2357–9

[5] Specifications are from the website of QMC Instruments (Cardiff, Wales) http://www.terahertz.co.uk/QMCI/qmc.html Similar detectors are also offered by Infrared Labs (Tucson, AZ).

[6] Santavicca D F, Reese M O, True A B, Schmuttenmaer C A and Prober D E 2007 Antenna-coupled niobium bolometers for terahertz spectroscopy *IEEE Trans. Appl. Supercond.* **17** 412–5

[7] Gershenzon E M, Gol'tsman G N, Karasik B S, Lugova G Ya, Serebryakova N A and Chinkova E V 1992 *Sverkhprovodimost (KIAE)* **5** 1129–40
Gershenzon E M, Gol'tsman G N, Karasik B S, Lugova G Ya, Serebryakova N A and Chinkova E V 1992 IR radiation detectors based on electronic heating of films made from conventional superconductors in the resistive state *Superconductivity* **5** 1126–37 (Engl. Transl.)

[8] Zmuidzinas J and Richards P L 2004 Superconducting detectors and mixers for millimeter and submillimeter astrophysics *Proc. IEEE* **92** 1597–616

[9] Specifications are from the website of Insight Product Co. (Newton, MA) http://www.insight-product.com/detect3.htm.

[10] Bendford D J, Gaidis M C and Kooi J W 2003 Optical properties of Zitex in the infrared to submillimeter *Appl. Opt.* **42** 5118–22

[11] Bin M, Benford D J, Gaidis M C, Buttgenbach T H, Zmuidzinas J, Serabyn E and Phillips T G 1999 A large throughput high resolution Fourier transform spectrometer for submillimeter applications *Int. J. Infrared Millim. Waves* **20** 383–400

[12] Evans G, Schmadel D C, Sushkov A B and Drew H D 2007 Silicon beamsplitter for Fourier transform spectroscopy at far infrared frequencies *Preprint* 0706.4302

[13] Skalare A, de Graauw Th and van de Stadt H 1991 A planar dipole array antenna with an elliptical lens *Microw. Opt. Technol. Lett.* **4** 9–12

[14] Rutledge D B, Neikirk D P and Kasilingam D P 1983 *Integrated Circuit Antennas Infrared and Millimeter Waves* vol 10, ed K J Button (New York: Academic) pp 1–90

[15] Dyson J D 1959 The equiangular spiral antenna *IRE Trans. Antennas Propag.* **13** 181–7

[16] Balanis C A 2005 *Antenna Theory: Analysis and Design* 3rd edn (Hoboken, NJ: Wiley) pp 611–8

[17] Beard M C, Turner G M and Schmuttenmaer C A 2000 Transient photoconductivity in GaAs as measured by time-resolved terahertz spectroscopy *Phys. Rev.* B **62** 15764–77

[18] Baxter J B and Schmuttenmaer C A 2006 Conductivity of ZnO nanowires, nanoparticles, and thin films using time-resolved terahertz spectroscopy *J. Phys. Chem.* **110** 25229–39

[19] Cooke D G, MacDonald A N, Hryciw A, Wang J, Li Q, Meldrum A and Hegmann F A 2006 Transient terahertz conductivity in photoexcited silicon nanocrystal films *Phys. Rev.* B **73** 193311

[20] Haran G, Sun W-D, Wynne K and Hochstrasser R M 1997 Femtosecond far-infrared pump-probe spectroscopy: a new tool for studying low-frequency vibrational dynamics in molecular condensed phases *Chem. Phys. Lett.* **274** 365–71

[21] Markelz A, Whitmire S, Hillebrecht J and Birge R 2002 THz time-domain spectroscopy of biomolecular conformal modes *Phys. Med. Biol.* **47** 3797–805

Erratum

In the first paragraph of section 4 (p. S400), the sentence

The antenna radiates power preferentially into the high dielectric silicon in proportion to the square root of the dielectric constant [14], so approximately 80% of the power should be coupled via the hyperhemispherical lens.

should be corrected to read

The antenna radiates power preferentially into the high dielectric silicon approximately in proportion to the dielectric constant to the power 3/2 [14].

Superconductor Science and Technology

100 μm